Milled-Si@C Composites as Potential Anode Materials for Li-ion Batteries

Hong Lv[1,], Sen Wang[1], Guanghui Zhang[1], Dabin Wang[2], Wei Zhou[1], Bing Li[1], Minzhe Xue[1], Cunman Zhang[1,*]*

[1] Clean Energy Automotive Engineering Center & School of Automotive Studies, 4800 Caoan Road, Tongji University, Shanghai 201804, China
[2] Australian Centre for Electromaterials Science, School of Chemistry, Monash University, Clayton, VIC 3800, Australia
*E-mail: lvhong@tongji.edu.cn, zhangcunman@tongji.edu.cn

Silicon (Si) has been identified as having high potential for lithium-ion battery anodes because of its ultrahigh capacity. However, its dramatic volume change in the process of lithiation/delithiation and its intrinsically poor electrical conductivity have severely inhibited its practical application. Herein, micron-sized Si alloys with carbon shells are prepared by high-energy ball milling coupled with an evaporation self-assembly method. A high and stable specific capacity of 850.5 mAh/g is achieved over 50 cycles and held at 650 mAh/g after 350 cycles with a coulombic efficiency >99.8%. The highly improved performance could be attributed to the unique microstructure of the as-synthesized composite materials in which crystalline Si nanoparticles are embedded in amorphous Si-M_2O_3 (M = Al and Si) matrix phases with a carbon shell on the surface, thereby achieving better buffering capacity and conductivity. The results we obtained could pave the way for using silicon as anodes for lithium-ion batteries.

1. INTRODUCTION

Li-ion batteries (LIBs) have been widely used in household information appliances, such as electric scooters, laptop computers, smartphones, and camcorders, for the last two decades. Energy crises and environmental pollution are forcing development in larger device applications, such as EVs, robots and electric power storage units, which require an increase in LIB mass capacities and energy densities [1]. In the case of 18650 Li-ion batteries, it is clear that developing materials with high capacity in the range of 1000–1200 mAh/g to replace carbonaceous anodes (372 mAh/g) is inevitable [2-4].

Metal-based anodes (such as Si, Al, Mg, Sn, and Sb) are regarded as the anodes with the most potential because of their high capacity and suitable working potential [5-9]. Their commercial usage has been hindered by a large volume change during lithiation/delithiation and their inherently poor electrical conductivity, leading to a rapid decline in capacity during cycle testing. Among those metals, Si shows the highest theoretical specific capacity (4200 mAh/g) because each Si atom can host 4.4 lithium atoms with the formation of a $Li_{22}Si_5$ alloy [10]. In addition to its excellent capacity, Si is the second most abundant element in the Earth's crust [11-15]. For these reasons, Si has received widespread attention as an anode material for LIBs. Unfortunately, the formation of successive Li–Si alloys gives rise to gradually larger volume expansions of the parent lattice. The 400% final volume expansion of the $Li_{22}Si_5$ alloy results in severe capacity fade due to material pulverization, active material loss, morphology and volume changes of the whole Si electrode, and the ongoing breakdown and formation of solid-electrolyte interphase (SEI) layers in the repeated cycles. Consequently, the above issues and the poor electrical conductivity of silicon lead to significant capacity decay and low coulomb efficiency, which limits the practical application of silicon materials [16]. To date, enormous amounts of research have been devoted to solving these problems by using different morphologies and structures of silicon materials, such as thin films, nanowires, nanotubes, nanosheets, and hollow structures [17]. Nevertheless, the undesirable side reactions and the reduced volumetric energy density caused by their large surface area severely hinder their practical use [18]. In addition, the large surface area of nanostructured Si often causes agglomeration during repetitive lithiation/delithiation processes [19]. Hence, further studies have focused on constructing Si-based nanostructure composites to control volume expansion and increase the electrical conductivity of Si anodes, thereby achieving high specific capacity, good calendar life and efficient charge–discharge capability for LIBs [20-23].

In this study, micron-sized silicon alloys consisting of crystalline Si nanoparticles embedded in amorphous silicon-M_2O_3(M = Al and Si) matrix phases were synthesized by high-energy ball milling [24]. Then, a carbon-coated micron-sized Si alloy core–shell nanocomposite (Si@C) was achieved by a facile evaporation self-assembly method [25]. The Si@C nanocomposite was designed and constructed to eliminate the undesired side effects resulting from volume expansion in the lithiation/delithiation process and fortify the electron transport pathway for the electrode. The obtained Si@C nanocomposite exhibited dramatically improved cycling performance with a stable high energy capacity and rate capability. It was demonstrated that ball-milling is a facile and effective route for achieving micro-sized Si alloy nanocomposites, and the resulting anodes revealed superior electrochemical performance to nanosized Si anodes. Owning to the safe and easy handling in this process, this technique allows the mass fabrication of micro-scale sized milled Si powder, which is crucial in practical applications for next-generation LIBs.

2. EXPERIMENTAL

2.1 Preparation of the milled Si powder

Commercial nanometric silicon (99.9%, 100 nm, KJ GROUP) powders were purchased as raw materials and commercial Al balls (99.9%, 2 and 5 mm, Changsha Tianchuang Powder Technology Co., Ltd) were used as received. First, the raw Si powders and 6 Al balls (three of 5 mm and three of 2

mm diameter) were added into a stainless-steel ball mill tank. The mass ratio of Al balls to powders was 5:1. Then, the powders were high-energy ball milled in a SPEX 8000 mixer for 5 h at room temperature. Second, the as-obtained powders and 20 stainless-steel balls (three of 5 mm and three of 2 mm diameter) were added into a stainless-steel ball mill tank. The mass ratio of stainless-steel balls to powders was 20:1. The ball mill stopped at regular intervals to keep the mill process at room temperature.

2.2 Preparation of the milled-Si@C nanocomposite

Carbon coated on the surface of the silicon material was synthesized by a typical method. Briefly, 2 g of the obtained milled Si powder was dispersed into 100 mL ethanol and sonicated for 1 h. Then, 50 mL resin alcohol solution (10 M) was added into the above suspension dropwise with constant stirring for 4 h. Then, the suspension was transferred into a vacuum rotary evaporator and operated at 100 °C for 2 h. Finally, the obtained powers were placed under heat treatment at 700 °C for 2 h under a nitrogen atmosphere with a heating rate of 5 °C/min.

2.3 Sample characterization

The X-ray diffraction patterns of the as-obtained samples were collected using a Bruker D8 Advance X-ray diffractometer (Bruker, Karlsruhe, Germany) with a Cu Kα radiation source (λ = 0.154056 nm). The morphological information was recorded by using a scanning electron microscope (SEM, FEI SIRION200) and high-resolution transmission electron microscopy (HRTEM, JEOL 2010F microscope). The chemical state of the elements in the samples was examined by X-ray photoelectron spectroscopy (XPS) measurements using a PHI 5000C ESCA System instrument (Petroleum Helicopters Inc) assembled with a monochromatic Al Kα X-ray source at 14.0 kV and 250 W. The spectra were corrected using the C 1s line at 284.6 eV, and the spectral curves were fitted by using Gaussian−Lorentzian type profiles (CasaXPS 2.3).

2.4 Electrochemical measurements

A slurry was formed using 70 wt% active materials, 10 wt% Super P (Kejing Star), 5 wt% graphite (Shanshan Technology), and 15 wt% sodium alginate (Sinopharm Chemical) dispersed into a certain amount of ultrapure water. The slurry was coated on Cu foil by the doctor blade method and dried in a vacuum oven at 75 °C for 8 h. The amount of the active materials loaded on the Cu foil was controlled at 2 mg/cm^2. Lithium foil and Celgard 2325 were used as the counter and the separator, respectively. The electrolyte was prepared using 1.0 M LiPF$_6$ (Tinci Materials) dissolved in dimethyl carbonate (DMC) and fluoroethylene carbonate (FEC) with a volume ratio of 4:1. Then, the types of CR2032 coin cells were assembled in MBraun glove boxes under argon atmosphere. The cyclic voltammograms (CVs) were measured in the range of 0.01 to 1 V (vs. Li/Li$^+$) by an electrochemical workstation (CHI660E, Shanghai) with a scan rate of 50 mV/s. The galvanostatic charge and discharge

measurements were recorded by using Land battery testers (CT2001A, Wuhan) in the potential range of 0.01-1.0 V (vs. Li/Li$^+$) at room temperature. Unless stated otherwise, the capacity in this study was calculated on the basis of the total mass of the prepared materials. Electrochemical impedance spectrum (EIS) measurements were performed in a frequency range from 100 kHz to 0.01 Hz at open circuit potential with an amplitude of 10 mV.

3. RESULTS AND DISCUSSION

Fig. 1 shows the XRD patterns of the as-received Si and the prepared milled-Si@C. The diffraction peaks of the as-received Si matched well with JCPDS no. 65-1060. The peaks located at 28.4, 47.3, 56.1, 69.1 and 76.4 correspond to the (111), (220), (311), (400) and (331) planes of Si, respectively (JCPDS no. 65-1060). For milled-Si@C, the pattern is similar to that of the as-received Si, and no other peaks appear, suggesting that the carbon layer is very thin. These peaks became much broader after the ball-milling process, representing milling-induced crystallite size reduction. Calculations with the Scherrer formula yielded 8.3 nm for the average crystallite size of the milled samples [26].
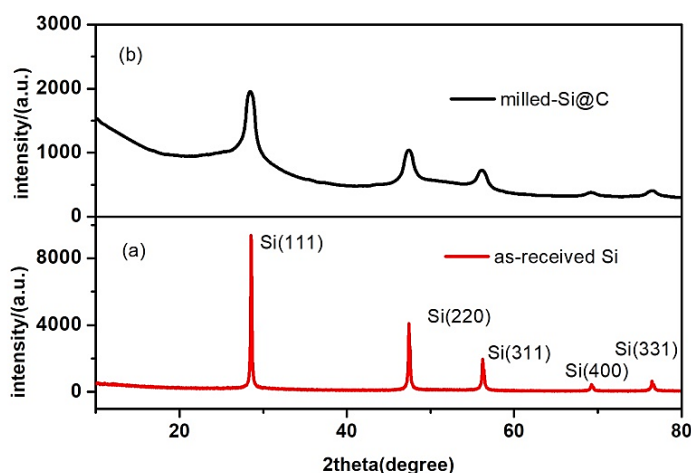

Figure 1. XRD patterns of the as-received Si and the prepared milled-Si@C

The chemical state of the milled-Si@C sample was further examined by XPS measurements. Fig. 2 shows the high-resolution spectrum for the Al 2p of milled-Si@C. The peak observed at 74.5 eV confirms the presence of Al_2O_3 [27], which originated from the interaction between Si particles and grinding balls during the high energy milling process. The very small amount of aluminium was oxidized in the unprotected atmosphere by the local heat produced by the collisions. The role of Al_2O_3 will be elaborated upon in the following section.
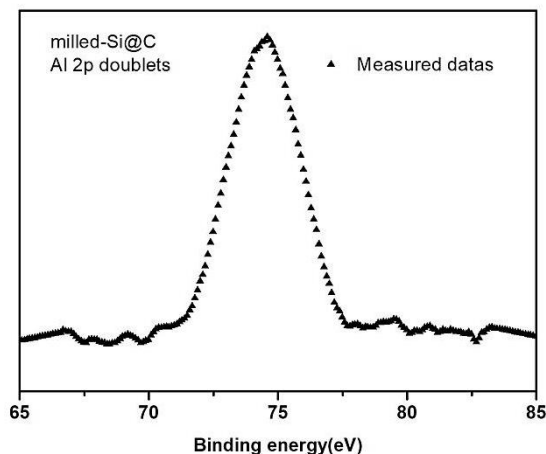
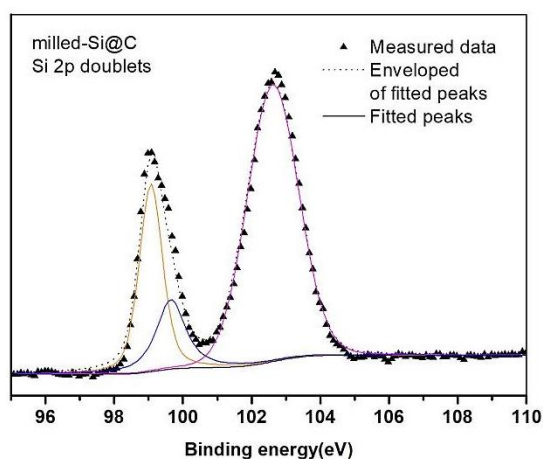**Figure 2.** XPS core-level Al 2p spectra of the milled-Si@C

Figure 3. XPS core-level Si 2p spectra of the milled-Si@C

The high-resolution XPS spectrum of Si 2p in milled-Si@C is shown in Fig. 3. The peak has been divided into two peaks corresponding to Si $2p_{3/2}$ (98.8 eV) and Si $2p_{1/2}$ (102.71 eV). Table 1 lists the binding energies, relative assignments and atomic concentrations of Si 2p. Additionally, the peaks at 98.8 eV and 102.71 eV confirm the existence of Si and Si oxide, and the ratio of Si to Si oxide peak areas is 30.5:69.5. The detected Si oxide could be ascribed to the elemental Si being oxidized in the high-energy ball mill process [28-30].

Table 1. XPS data of the core-level Si 2p spectra in the milled-Si@C sample

Binding energy (eV)	Assignment	Concentration (%)
98.79, 99.62	Si-Si	69.5
102.71	SiO_2	30.5

The morphologies of the as-received Si and milled Si were investigated by SEM. The as-received Si sample (Fig. 4a) consisted of a series of differently sized particles with irregular shapes, while the milled Si powder was composed of particle agglomerates (Fig. 4b) that could be attributed to the repeated cold welding/fracturing processes caused by the strong ball-to-powder collisions; this powder then achieved a balanced state during ball-milling that is closely related to the mechanical properties of the material [24]. Fig. 4c highlights the agglomerated Si powders being made of nanoscale plate-like grains.
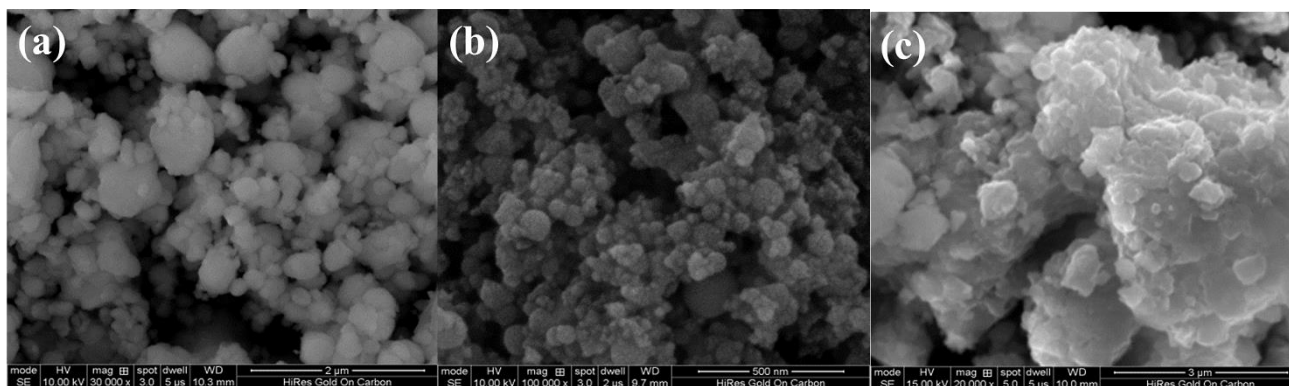

Figure 4. SEM images of the as-received (a) and milled Si (b, c) powders

The morphologies of the milled-Si@C nanocomposite were further analysed by TEM and HRTEM. As shown in Fig. 5a, it is easy to observe the detailed microstructure of the milled-Si@C nanocomposite. The large particle sizes confirm the particle agglomerates of Si after milling. The darker dots homogeneously distributed on the surface of the milled-Si@C nanocomposite are confirmed to be tiny Al_2O_3 nanocrystals by HRTEM (Fig. 5b) and the corresponding electron diffraction pattern (Fig. 5c). The HRTEM image in Fig. 5b clearly shows the lattice fringes for Al_2O_3 and Si. Fig. 5c exhibits the characteristic reflections of crystalline Al_2O_3 (JCPDS no. 46-1212) [31] and the presence of superlattice reflections at (104) and (012). Fig. 5d reveals the characteristic reflections of crystalline Si (JCPDS no. 27-1402) and the presence of superlattice reflections at (220), (111) and (311) [32-33]. According to the TEM and HRTEM analysis, the crystalline Si nanoparticles embedded in the amorphous SiO_2 matrix together with a few Al_2O_3 nanocrystals could act as the additional buffer/spacer during the volume changes of the active Si phase. The unique microstructure could also enhance the mechanical strength of the material, providing potentially better cycling performance during a long-term charge/discharge process.
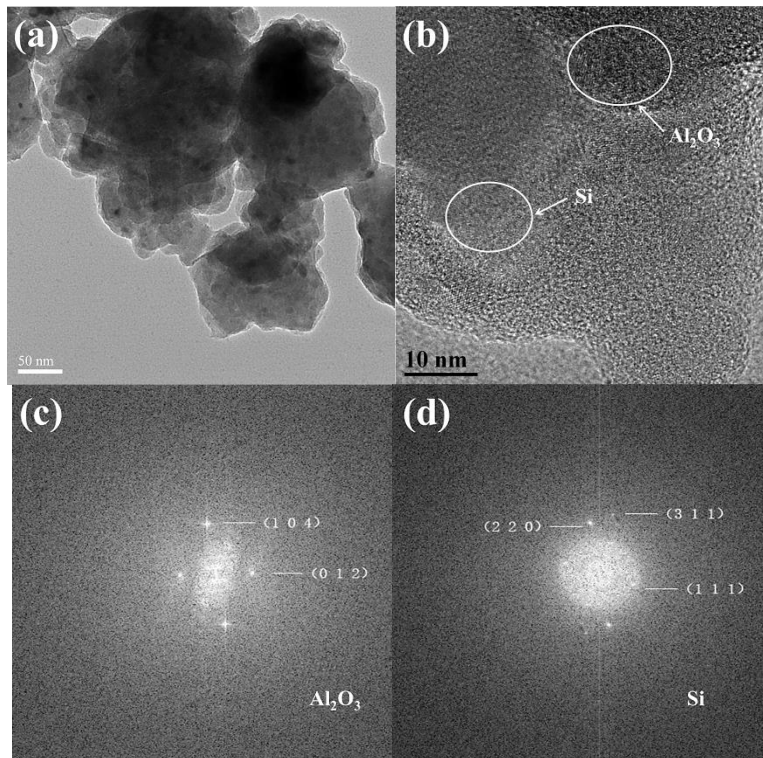
Figure 5. TEM image (a), HRTEM image (b) and the corresponding electron diffraction pattern of Al₂O₃ (c) and the milled-Si@C (d)
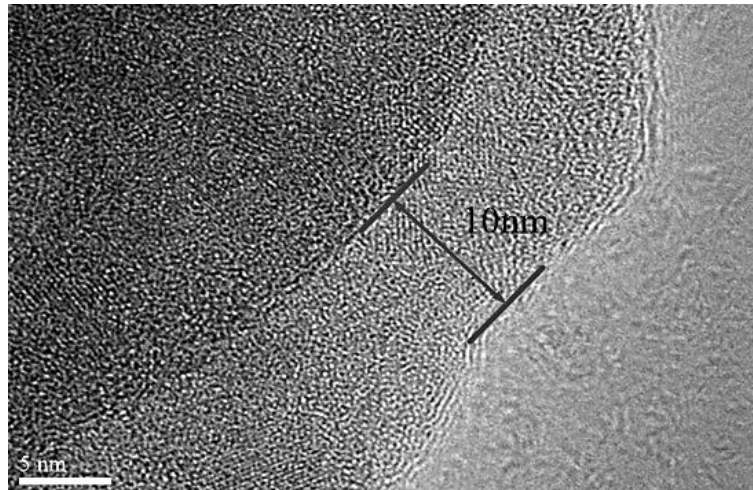

Figure 6. HRTEM image of the milled-Si@C

The coated carbon layer was observed by HRTEM. As shown in Fig. 6, the carbon layer is approximately 10 nm thick and covers the surface of the milled Si particles. The thin layer could not only protect the Si particles from being pulverized during the long-term cycling process but also provide better conductivity of the material. Consequently, the composite could deliver much better stability and rate capability.

The cyclic voltammograms of the as-received Si and milled-Si@C electrodes were measured to analyse the electrode electrochemical properties. As shown in Fig. 7, the cathodic peak loaded at 0.2 V

was not observed during the lithiation process in the first cycle for both the as-received Si (Fig. 7a) and milled-Si@C electrodes (Fig. 7b), indicating that the crystalline Si transformed to amorphous Si. The observed anodic peaks at ~0.42 and ~0.57 V are attributed to the delithiation action of the material. For milled-Si@C, the peaks at ~0.42 V and ~0.57 V were much broader than those of the as-received Si, suggesting that the two-phase process is smoothed [34]. In addition, the increased intensity of the two peaks at the second cycle could be ascribed to the activation process in the initial cycles.
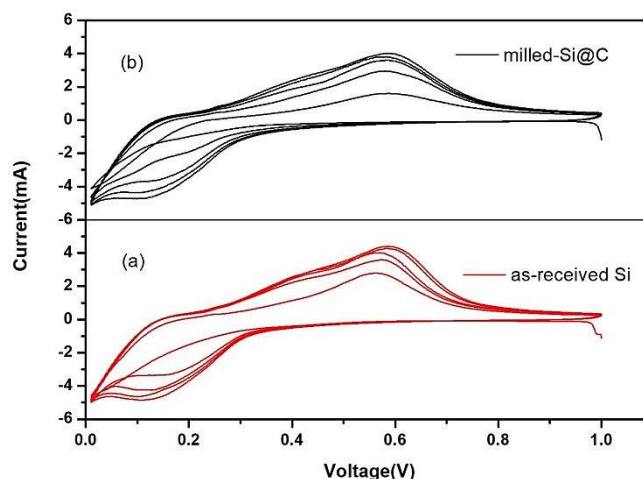

Figure 7. The CV curves of the as-received Si and the prepared milled-Si@C electrodes

The first cycle voltage curve (Fig. 8a) clearly shows a well-defined discharge plateau at ~0.1 V for the as-received Si electrode, which is consistent with the alloying behaviour for crystalline silicon [35]. Unlike the as-received Si electrode, the milled-Si@C electrode (Fig. 8b) shows a monotonic variation in both the charge and discharge process without any well-defined plateaus. This behaviour reflects the decreased grain size after ball-milling, which is consistent with the XRD data.
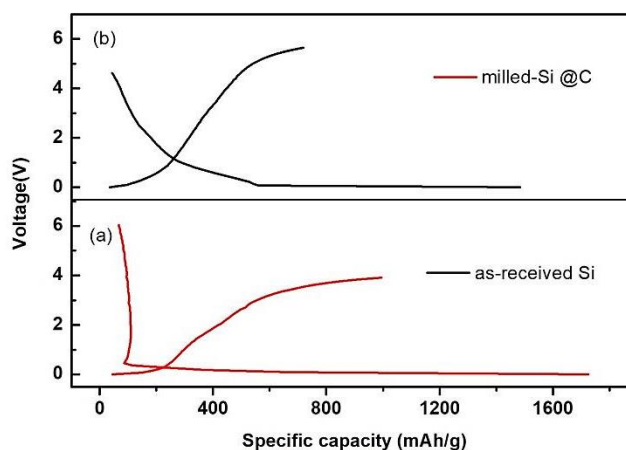

Figure 8. The voltage curve of the as-received Si and the prepared milled-Si @C electrodes

Galvanostatic charge/discharge cycling tests of the as-received Si, milled Si and milled-Si@C electrodes were carried out. As shown in Fig. 9, all the samples were tested at C/20 for the first cycle and C/3 for the rest. It can be seen that the as-received Si electrode reveals a high initial discharge

capacity (3167.3 mAh/g) but experiences fast capacity fading (losing the ability to store lithium after 20 cycles). This behaviour could be attributed to the large volume expansion of silicon in the process of lithiation/delithiation. In the case of the milled Si and milled-Si@C electrodes, a superior reversible specific capacity of 620.5 and 850.5 mAh/g, respectively, is achieved over 50 cycles; most importantly, 650 mAh/g is retained after 350 cycles for the milled-Si@C sample. The results indicate that the Al ball milling could obviously enhance the stability performance, and the coated carbon layer could effectively buffer the volume expansion of silicon and relax the internal stress, thereby enormously enhancing the cycling stability for the Si electrodes. Al_2O_3 coming from the oxygenated Al has very high mechanical strength, which could prevent the Si particles from being broken by the internal stress produced during the charge/discharge process [36].

Although the large capacity declines occur from the first to the third cycle, it becomes apparently stable afterwards. The coulombic efficiency of the milled Si sample at the first and second cycles is 77.5% and 93.0%, respectively, while similar numbers are observed for the milled-Si@C, reaching a steady state very quickly and delivering nearly 100% coulombic efficiency for the following cycles.
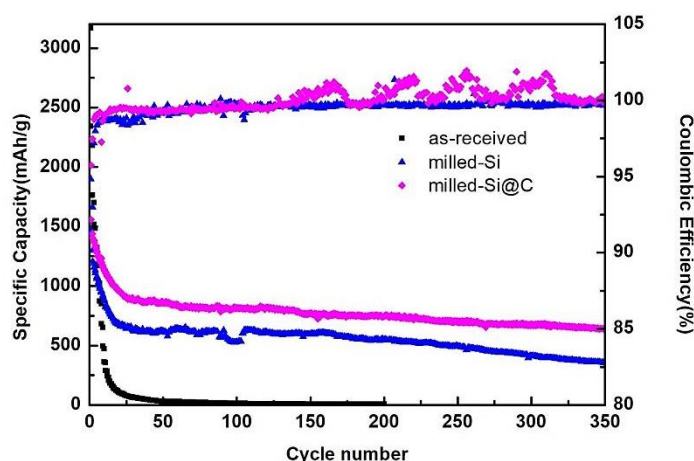

Figure 9. Cycling tests of the as-received Si, milled Si and milled-Si@C electrodes

Table 2. Electrochemical performance comparison of Si-based anode electrodes for LIBs

Materials	Reversible capacity (mAh g^{-1})	Initial discharge/charge specific capacity (mAh g^{-1})	Ref.
SiO$_x$@C	630 (150th)	1160/820	37
3D porous Si	755 (50th)	1906/–	38
Silicon oxide-carbon	601(100th)	1055/458	39
SiO$_2$@C/MWNT	557 (40th)	991/615	40
Milled-Si@C	650 (350th)	1690/850.5	This work

The rate capability of the prepared milled-Si@C electrode measured at different current densities was examined to further study the electrode's electrochemical performance. As shown in Fig. 10, the discharge specific capacity of the milled-Si@C electrode changes from 850.5 to 213.2 mAh/g with the current density increasing from C/3 to 10/3C, indicating a declining tendency. When the C-rate turns back to C/10, the capacity remains at 850.5 mA/g, indicating good recoverability of the milled-Si@C electrode. This could be ascribed to the enhancement of the electrical conductivity because of the well-designed carbon layer. Furthermore, the electrochemical performance comparison of Si-based anode electrodes for LIBs was investigated, and the results are listed in Table 2.
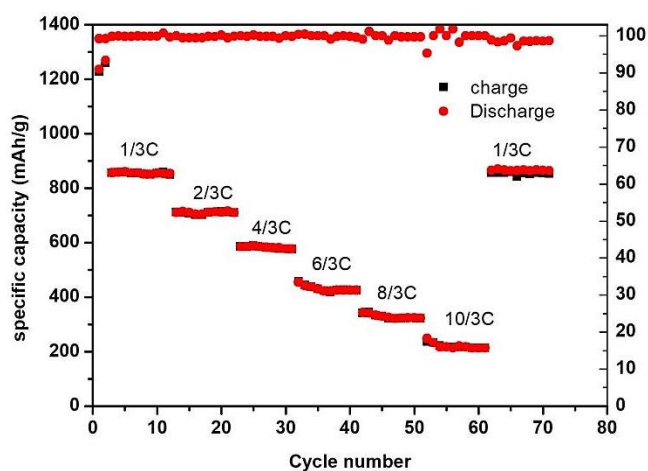

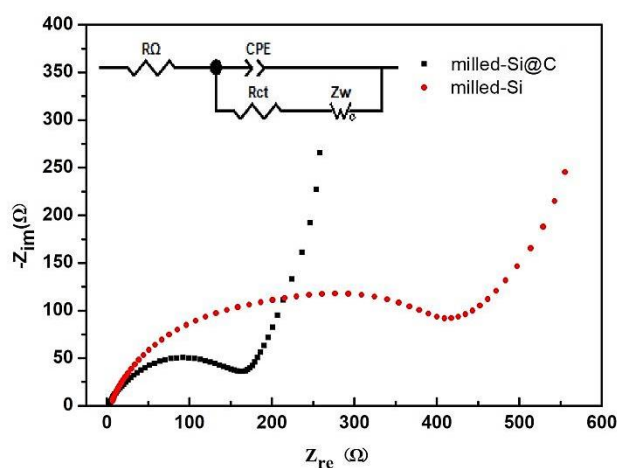**Figure 10.** The rate performance of the prepared milled-Si@C electrode

Figure 11. Nyquist plots of the milled Si and milled-Si@C electrodes and the equivalent circuit.

EIS Nyquist plots of the milled Si and the milled-Si@C electrodes were studied. As displayed in Fig. 11, the EIS Nyquist plots show a smaller charge-transfer resistance with the milled-Si@C in comparison to the milled Si. Additionally, the appropriate equivalent circuit for the measured EIS Nyquist plots was fit to analyse the key kinetic parameters. The equivalent circuit is shown in the inset

of Fig. 11. R_Ω is the ohmic resistance of the whole cell, and R_{ct} is the charge transfer resistance between the solution interface and electrodes. CPE is used to interpret the deviation from the ideal capacitor behaviour. Z_w is the diffusion resistance between the cell components, separator and electrolyte. According to the fitted results, R_Ω is 4.5 Ω for both samples, which suggests the good condition of the cells. In addition, the R_{ct} of the milled-Si@C decreases dramatically from 400 Ω to 145 Ω with the carbon coating. It is evident that the carbon layer on the surface of Si plays a pivotal role in improving electron transfer and electronic conductivity.

4. CONCLUSION

A milled-Si@C core–shell nanocomposite was successfully prepared by high-energy ball milling and evaporation self-assembly. From the characterization, it was confirmed that micron-sized silicon alloys were embedded in amorphous silicon-M_2O_3 (M = Al and Si) matrix phases and surrounded by a 10 nm thick carbon layer. Amorphous silicon, Al_2O_3 and Si_2O_3 successfully suppressed the volume changes of Si in the process of lithiation/delithiation, and the surrounding carbon shell provided continuous electron transport routes, which improved the electrical conductivity. For the milled-Si@C electrode, an excellent reversible specific capacity of 850.5 mAh/g was obtained over 50 cycles; 650 mAh/g was still retained after 350 cycles, showing good recoverability; and the R_{ct} between the solution interface and electrodes was reduced by 255 Ω. Furthermore, the high-energy ball-milling method was facile and controllable, representing a potential pathway to achieve high-performance silicon-based anode materials for LIBs.

References

1. J. Liu, Z. Bao, Y. Cui, E.J. Dufek, J.B. Goodenough, P. Khalifah and J.-G. Zhang, *Nat. Energy*, 4 (2019) 180.
2. R. Mo, F. Li, X. Tan, P. Xu, R. Tao, G. Shen, X. Lu, F. Liu, L. Shen, B. Xu, Q. Xiao, X. Wang, C. Wang, J. Li, G. Wang and Y. Lu, *Nat. Commun.*, 10 (2019) 1474.
3. M. Ren, F. Li, W. Liu, M. Li, G. Li, J. Hei, L. Su and L. Wang, *ChemElectroChem*, 4 (2017) 2862.
4. C. Erk, T. Brezesinski, H. Sommer, R. Schneider and J. Janek, *ACS Appl. Mater. Inter.*, 5 (2013) 7299.
5. H. Ying and W. Q. Han, *Adv. Sci.,* 4 (2017) 1700298.
6. Y. Tang, Y. Zhang, J. Deng, J. Wei, H. L. Tam, B. K. Chandran, Z. Dong, Z. Chen and X. Chen, *Adv. Mater.*, 26 (2014) 6111.
7. T. Leisegang, F. Meutzner, M. Zschornak, W. Münchgesang, R. Schmid, T. Nestler, R. A. Eremin, A. A. Kabanov, V. A. Blatov and D. C. Meyer, *Front. Chem.*, 7 (2019) 10.
8. X. Feng, D. Ren, S. Zhang, X. He, L. Wang and M. Ouyang, *Int. J. Electrochem. Sci.,* 14 (2019) 44.

9.   Y. Idota, T. Kubota, A. Matsufuji, Y. Maekawa and T. Miyasaka, *Science*, 276 (1997) 1395.
10. Y. Jin, B. Zhu, Z. Lu, N. Liu and J. Zhu, *Adv. Energy Mater*., 7 (2017) 1700715.
11. A. F. Gonzalez, N. Yang and R. Liu, *J. Phys. Chem.* C, 121 (2017) 27775.
12. F. Men, Y. Yang, Y. Shang, H. Zhang, Z. Song, Y. Zhou, X. Zhou and H. Zhan, *J. Power Sources* 401 (2018) 354.
13. X. Chang, Z. Xie, Z. Liu, X. Zheng, J. Zheng and X. Li, *Nano Energy* 41 (2017) 731.
14. D. Farhat, J. Maibach, H. Eriksson, K. Edström, D. Lemordant and F. Ghamouss, *Electrochim. Acta,* 281 (2018) 299.
15. K. A. Hays, B. Key, J. Li, D. L. Wood and G. M. Veith, *J. Phys. Chem*. C, 122 (2018) 189746.
16. A. G. Kannan, S. H. Kim and H. S. Yang, *RSC Adv*., 6 (2016) 25159.
17. W. Hui and C. Yi, Nano *Today,* 7 (2012) 414.
18. J. R. Szczech and J. Song, *Energy Environ. Sci*., 2010, 4, 56-72.
19. J. Wang, X. Meng, X. Fan, W. Zhang, H. Zhang and C. Wang, *ACS Nano,* 96 (2015) 6576.
20. B. C. Yeo, H. Jung, H. W. Lee, K. Yun, H. Kim, K. R. Lee and S. S. Han, *J. Phys. Chem*. C 121 (2017) 23268.
21. Y. S. Choi, J. H. Park, J. P. Ahn and J. C. Lee, *Sci. Rep*., 7 (2017) 14028.
22. J. Zhao, Z. Lu, N. Liu, H.-W. Lee, M. T. McDowell and Y. Cui, *Nat. Commun*. 5(2014) 5088.
23. S. Kim and A. Manthiram, *J. Mater. Chem*. A, 3 (2015) 2399.
24. M. Gauthier, D. Mazouzi, D. Reyter, B. Lestriez, P. Moreau, D. Guyomard and L. Roué, *Energy Environ. Sci.,* 6 (2013) 2145.
25. Y. Meng, D. Gu, F. Zhang, Y. Shi, H. Yang, Z. Li, C. Yu, B. Tu and D. Zhao, *Angew. Chem. Int. Edit.,* 44 (2005) 7053.
26. S. Wang, J. Yoon, G. Kim, D. Huang, H. Wang and A. J. Jacobson, *Chem. Mater*. 22 (2010) 776
27. C. Wei, G. Zhang, Y. Bai, D. Yan, C. Yu, N. Wan and W. Zhang, *Solid State Ionics* 272 (2015) 133.
28. F. Priante, M. Salim, L. Ottaviano and F. Perrozzi, *Nanotechnology* 29 (2018) 075704.
29. X. Zhang, M. Huang, C. Yang, G. Dai and J. Huang, *Mater. Chem. Phys*., 201 (2017) 302.
30. K. Johansson and E. Lewin, *J. Alloy. Compd*. 738 (2018) 515.
31. J. Lin, G. Ran and P. Lei, *Metals,* 7 (2017) 67.
32. A. G. Kannan, S. H. Kim, H. S. Yang and D. Kim, *RSC Adv.,* 6 (2016) 25159.
33. H. Li, X. Huang, L. Chen, G. Zhou, Z. Zhang, D. Yu, Y. J. Mo and N. Pei, *Solid State Ionics* 135 (2000) 181.
34. M. Gauthier, J. Danet, B. Lestriez, L. Roue, D. Guyomard and P. Moreau, *J. Power Sources*, 227 (2013) 237.
35. J. Feng, Z. Zhang, L. Ci, W. Zhai, Q. Ai and S. Xiong, *J. Power Sources*, 287 (2015) 177.
36. S. Yoon and A. Manthiram, *Chem. Mater*., 21 (2009) 3898.
37. M. Li, Y. Zeng, Y. Ren, C. Zeng, J. Gu and X. Feng, *Mater. Lett.* 288 (2015) 53.
38. Q. T. Wang, L. J. Han, X. Zhang, J. Li, X. Z. Zhou and Z. Q. Lei, *Mater. Lett.* 185 (2016) 558.
39. J. Y. Kim, D. T. Nguyen, J. S. Kang and S. W. Song, *J. Alloys Compd.* 633 (2015) 92.
40. Y. Zhao, Z. Liu, Y. Zhang, A. Mentbayeva, X. Wang, M. Y. Maximov, B. Liu, Z. Bakenov and F. Yin, *Nanoscale Res. Lett.* 12 (2017) 459.